GEOPHYSICS, VOL. 87, NO. 3 (MAY-JUNE 2022); P. V193–V203, 23 FIGS.
10.1190/GEO2021-0167.1

Wavelet estimation and nonstretching NMO correction

Hanlin Sheng[1], Xinming Wu[1], and Bo Zhang[2]

ABSTRACT

Normal-moveout (NMO) correction is an important step applied to common-midpoint (CMP) gathers for subsequent stacking. However, conventional NMO correction methods often suffer from the problem of NMO stretching, which nonlinearly increases with offsets and decreases with zero-offset traveltime. The NMO stretching can be quantified by frequency distortion, so stretching is confined mainly to large offsets and shallow times. To solve this problem, we have proposed a wavelet-based method with the following four steps. First, we estimate a wavelet from the CMP gather by using the NMO stretching appearing in the conventional NMO correction. Second, we deconvolve the original CMP gather based on the estimated wavelet. This step of removing the wavelet from the CMP gather is helpful for the next steps of NMO velocity scan and NMO correction. Third, we apply an improved NMO correction to the deconvolved CMP gather and obtain flattened reflectivities. Finally, we convolve the flattened and deconvolved gather with the estimated wavelet back to obtain an NMO-corrected gather without stretching artifacts. In our method, by using a deconvolved CMP gather, we are able to calculate a high-resolution semblance velocity spectrum that benefits from the NMO velocity picking. In addition, applying the NMO correction to the deconvolved CMP gather, instead of the original gather, is helpful in reducing the NMO stretching related to the wavelet distortion. Tests on synthetic and field data find that our new NMO correction method can estimate an accurate seismic wavelet and obtain an NMO-corrected gather without NMO stretching. Reducing the NMO stretching can significantly improve the resolution of shallow layers at far offsets and preserve the spectral bandwidth.

INTRODUCTION

Normal-moveout (NMO) correction converts a recorded common-midpoint (CMP) gather to a kinematically equalized gather in which the seismic event moveout over offset is eliminated. Such a flattened gather then can be stacked over offset to obtain a seismic image. However, conventional NMO correction methods often generate the artifacts of stretching in the corrected or flattened gather. Such stretching not only reduces the resolution of the flattened gather but also squeezes the frequency spectrum range. Buchholtz (1972) first describes the wavelet distortion while performing NMO correction as NMO stretching. The magnitude of the NMO stretching depends on offset, two-way traveltime, and a velocity model used for the NMO correction. The NMO stretching is especially significant at far offsets and early traveltimes. In addition, the extent of spectral compression is correlated with the extent of NMO stretching while performing NMO correction (Dunkin and Levin, 1973). Barnes (1992) shows how the instantaneous frequency and instantaneous power domain vary over time. Miller (1992) points out that the effect of NMO stretching at high frequencies can be reduced by muting the CMP gather properly. However, this muting method often results in the loss of data and lowers the resolution of the CMP gather (Noah, 1996).

One way to reduce the NMO stretching is to use nonhyperbolic moveout to flatten the CMP gather (Dix, 1955; Bolshykh, 1956; de Bazelaire, 1988; Castle, 1994; de Bazelaire and Viallix, 1994; Alkhalifah, 1997, 1998; Ursin and Stovas, 2006; Fomel and Stovas, 2010; Abedi and Riahi, 2016). Such nonhyperbolic moveout

Manuscript received by the Editor 12 March 2021; revised manuscript received 9 February 2022; published ahead of production 2 March 2022; published online 29 March 2022.
[1]University of Science and Technology of China, School of Earth and Space Sciences, Laboratory of Seismology and Physics of Earth's Interior, Hefei, China and University of Science and Technology of China, Mengcheng National Geophysical Observatory, Hefei, China. E-mail: hanlins@mail.ustc.edu.cn; xinmwu@ustc.edu.cn (corresponding author).
[2]The University of Alabama, Geological Sciences, Tuscaloosa, Alabama, USA. E-mail: bzhang33@ua.edu.

corrections generate more accurate velocity analysis and obtain a higher resolution at large offsets. Even though the nonhyperbolic moveout correction methods improve the NMO correction results, the NMO stretching still remains.

Block move sum (BMS) (Rupert and Chun, 1975) is another type of method to deal with NMO stretching, which separates the CMP gather into many blocks and applies a uniform NMO correction for each block. However, discontinuity artifacts often occur at the junction of the blocks while performing the BMS method. Similarly, Shatilo and Aminzadeh (2000) present a constant normal moveout (CNMO) method to correct the CMP in a limited time interval. The CNMO method can reduce higher frequency compression at far offsets due to the NMO stretching. Unfortunately, it typically requires high-accuracy velocities for NMO correction. To reduce the discontinuity, Brouwer (2002) improves the BMS method by using a coherence filter. Masoomzadeh et al. (2010) point out the impact of blocks on NMO: small blocks bring stretching distortion, whereas large blocks produce image discontinuity. They use isomoveout curves to implement multiblock constant moveout correction.

Lichman (1999) proposes an NMO supplementary method called phase-moveout correction, which replaces the phase spectrum of the nonminimum-offset trace with the minimum-offset one. This method is equivalent to moving the arrival time of all traces to the corresponding initial time of the minimum-offset trace. However, this method is not stable, and it depends on the quality of the recorded data because the phase spectrum of the minimum offset trace depends on the signal-to-noise ratio (S/N) of the near-offset traces. Hicks (2001) reduces NMO stretching using a combination of the Radon transform and spatial Fourier transform.

Trickett (2003) proposes a stretch-free stack method in which the NMO correction is implicitly performed. However, this method is not beneficial to amplitude-variation-with-offset (AVO) analysis as an NMO-corrected gather is not explicitly computed. Hilterman and Schuyver (2003) propose a seismic wide-angle processing method, in which the traveltime is calculated on a target reflection model in the common-offset domain. This method works well for the target layer corresponding to the reflectivity model, but it cannot flatten layers that have reflection arrivals different from the target reflector. Perroud and Tygel (2004) propose a nonstretching NMO correction method for high-resolution seismic data. Their method continuously adjusts the velocity and time of the reflection layers through velocity analysis, but it also will generate NMO stretching among the interval between identified reflectors.

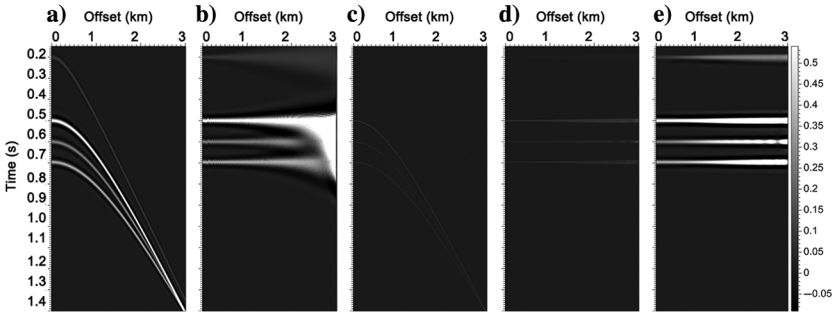

Figure 1. (a) A synthetic gather with multiple crossing hyperbolic trajectories is corrected by using (b) a conventional NMO method and our method in which we first deconvolve (c) the synthetic gather and then apply (d) the improved NMO correction and convolve the wavelet back onto the data to obtain (e) the finally corrected gather without stretching.

Some iterative methods also are proposed to reduce NMO stretching and restore the wavelet distortion (Zhang et al., 2012). Biondi et al. (2014) propose an iterative procedure of partial NMO correction and Wiener shaping filter. These iterative methods can handle the NMO stretching with the implementation of wavelets, but they all need to perform NMO correction at each iteration, which can be computationally expensive.

In this paper, we first introduce the concept of NMO stretching and then propose a new method for wavelet estimation using NMO stretching. Using the calculated wavelet, we present a new NMO correction method called *wavelet NMO (WNMO)* to reduce NMO stretching. In our WNMO method, we apply a one-sample length BMS method to the deconvolved CMP gather with an estimated wavelet and then convolve the wavelet back onto the data to obtain the final nonstretching NMO-corrected gather. In summary, by applying the entire workflow of our method, we are able to estimate a seismic wavelet, compute a high-resolution velocity-semblance spectrum for picking accurate NMO velocities, and obtain an NMO-corrected gather without NMO stretching artifacts. We demonstrate our method on three different synthetic seismic data sets; the first example contains multiple crossing hyperbolic events, the second example is generated with linearly increasing velocities, and the third example is generated with the Marmousi velocity model. We also apply our method to real seismic data sets to demonstrate its effectiveness in estimating an accurate seismic wavelet and removing stretching artifacts in NMO correction.

CONVENTIONAL NMO CORRECTION

To illustrate the NMO correction, we use a synthetic example with a simple velocity model that contains four layers of constant velocities of 2.25, 2.7, 2.9, and 3.2 km/s, respectively. From this velocity model, we generate the CMP gather in Figure 1 by using the following well-known traveltime equation (Dix, 1955):

$$t(t_0, x) = \sqrt{t_0^2 + \frac{x^2}{V^2(t_0)}}, \tag{1}$$

where t_0 represents two-way traveltime at zero-offset, $V(t_0)$ represents root-mean-square (rms) velocity, and x represents offset. Taner and Koelher (1969) introduce the NMO correction to flatten the curved events as follows:

$$\begin{aligned}\Delta t_{\mathrm{NMO}} &= t(t_0, x) - t_0 \\ &= \sqrt{t_0^2 + \frac{x^2}{V^2(t_0)}} - t_0,\end{aligned} \tag{2}$$

where the NMO correction Δt_{NMO} is expressed by the hyperbolic traveltime $t(t_0, x)$ minus zero-offset traveltime t_0. With the calculated NMO correction for every sample, we expect to laterally align seismic events by using the zero-offset trace as a reference. However, traditional NMO correction methods often introduce stretching artifacts in the corrected gather, especially at large offsets and when correction trajectories cross (Buchholtz, 1972; Dunkin and Levin, 1973), as shown in Figure 1b. The NMO stretch-

ing effect reduces the resolution of stacking the corrected CMP gather especially in the high offset-depth ratio portion of the data (Perez and Marfurt, 2007). In addition, NMO stretching downshifts the frequency spectrum. One method to deal with the NMO stretching is to mute out the data at far offsets and early traveltimes in which the NMO stretching is most significant (Miller, 1992; Noah, 1996). However, the muted far-offset data can be helpful in the AVO analysis and full-waveform inversion (Drufuca and Mazzotti, 1995; Roberts, 2000; Downton and Ursenbach, 2006; Prieux et al., 2013).

WNMO CORRECTION

We develop a new workflow to reduce NMO stretching and estimate a wavelet for the input CMP gather. This new workflow contains two main processes: first, we use the NMO stretching to estimate a wavelet, and second, we use the estimated wavelet to reduce the NMO stretching by using a proposed WNMO correction method. The results of each step in our workflow (Figure 2) are visually displayed for better understanding in Figure 3. The blue arrows indicate the process of estimating a wavelet through NMO stretching, whereas the red arrows indicate the process of our nonstretching NMO correction.

Wavelet estimation through NMO stretching

We first introduce our process of wavelet estimation denoted by the blue arrows in Figure 3. Before introducing the wavelet-estimation algorithm, we define some notations used throughout this algorithm. We use column vectors **g**, **h**, and **a** to represent one trace in the input gather $f(x,t)$, wavelet $h(t)$, and inverse wavelet $a(t)$, respectively, and define the traditional NMO correction as an operator **N**.

In our wavelet-estimating algorithm, we first correct the input CMP gather **g** with the traditional NMO correction **N** to obtain the NMO-corrected trace: **Ng** (one trace in Figure 3b) in which the NMO stretching occurs. Then, we laterally balance the amplitude and stack the traces in **Ng** and replicate the stacked trace to obtain the reference trace $d(t)$ denoted by **d** (one trace in Figure 3c). The balance operation aims to reduce the distraction of AVO effect when estimating the wavelet. Meanwhile, we can subtract the traditional NMO-corrected gather **Ng** from the reference one **d** to obtain the NMO stretching $\mathbf{s} = \mathbf{d} - \mathbf{Ng}$ (Figure 3d).

To simplify the expression of our algorithm, here we illustrate an inverse wavelet **a** with only three coefficients. (We actually use more coefficients to represent an inverse wavelet in practice.) Then, we can write a deconvolved gather as the convolution of the inverse wavelet **a** and the gather **g** as follows:

$$\mathbf{Ag} = \begin{bmatrix} a_0 & 0 & 0 & 0 & 0 \\ a_1 & a_0 & 0 & 0 & 0 \\ a_2 & a_1 & a_0 & 0 & 0 \\ 0 & a_2 & a_1 & a_0 & 0 \\ 0 & 0 & a_2 & a_1 & a_0 \end{bmatrix} \begin{bmatrix} g_0 \\ g_1 \\ g_2 \\ g_3 \\ g_4 \end{bmatrix}, \tag{3}$$

where **A** is a Toeplitz matrix. The columns of **A** are delayed copies of the inverse wavelet **a** and g_i ($i = 0, 1, 2, \ldots$) represents the ith sample of a trace **g**. Because the convolution is commutative, equation 3 can be equivalently written as

$$\mathbf{Ga} = \begin{bmatrix} g_0 & 0 & 0 \\ g_1 & g_0 & 0 \\ g_2 & g_1 & g_0 \\ g_3 & g_2 & g_1 \\ g_4 & g_3 & g_2 \end{bmatrix} \begin{bmatrix} a_0 \\ a_1 \\ a_2 \end{bmatrix}, \tag{4}$$

where **G** is a Toeplitz matrix with delayed copies of **g**. Therefore, we have the equation $\mathbf{Ag} = \mathbf{Ga}$. Assuming that a seismic trace is the convolution of a reflectivity model and a wavelet, we can convolve **g** with **A** to obtain a deconvolved trace **Ag**, which can be treated as the reflectivity trace. Here, we assume that the wavelet is invariant in time and space, which is not necessarily true in practice. One may use more sophisticated methods such as the least-squares blind deconvolution (Xu et al., 1995) and the sparse multichannel blind deconvolution method (Kazemi and Sacchi, 2014) to estimate the wavelet and compute the deconvolution. However, the main pur-

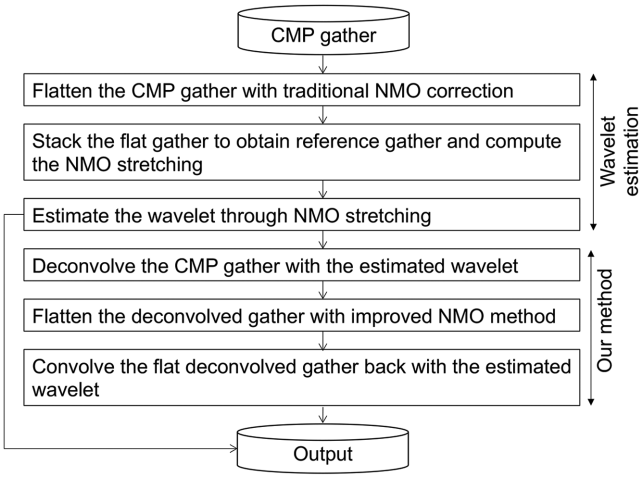

Figure 2. In this workflow, we show how to estimate the wavelet and improve NMO correction.

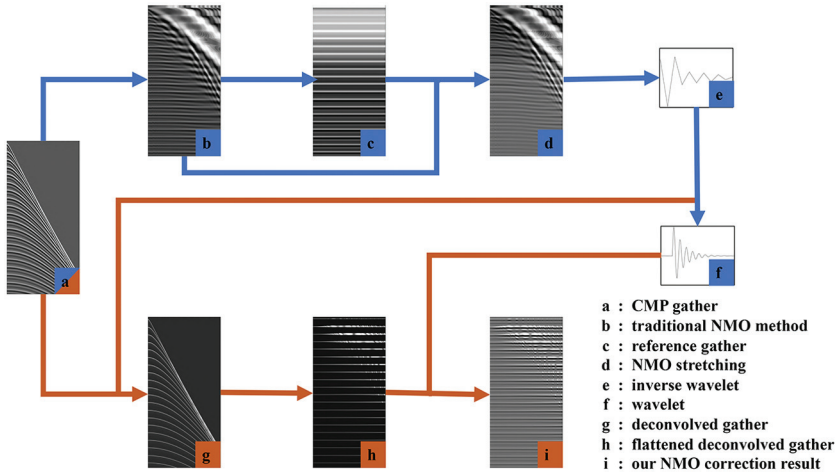

Figure 3. In this figure, we visually show the results of every step in our workflow.

pose of the deconvolution process in our workflow is to reduce the NMO stretching. Examples show that the simple deconvolution method with an invariant wavelet is sufficient for the purpose. More importantly, such a simple deconvolution is easy to implement and is computationally efficient.

After computing a deconvolved trace **Ag**, we can then apply NMO correction **N** to **Ag** to remove the NMO and obtain a flattened and deconvolved trace **NAg**. We can further convolve the wavelet **H** back to obtain an ideal NMO correction trace **HNAg**, which is expected to be equal to the reference NMO-corrected trace **d**:

$$\mathbf{d} = \mathbf{HNAg}. \tag{5}$$

We multiply both sides of equation 5 by **A** simultaneously to obtain the following equation:

$$\mathbf{Ad} = \mathbf{AHNAg}. \tag{6}$$

Note that $\mathbf{AH} = \mathbf{I}$, $\mathbf{Ad} = \mathbf{Da}$, and $\mathbf{Ag} = \mathbf{Ga}$, so that

$$\mathbf{Da} = \mathbf{NGa} \tag{7}$$

or

$$(\mathbf{D} - \mathbf{NG})\mathbf{a} = \mathbf{0}. \tag{8}$$

The matrix form of equation 8 is as follows:

$$\begin{bmatrix} d_0 - Ng_0 & 0 & 0 \\ d_1 - Ng_1 & d_0 - Ng_0 & 0 \\ d_2 - Ng_2 & d_1 - Ng_1 & d_0 - Ng_0 \end{bmatrix} \begin{bmatrix} a_0 \\ a_1 \\ a_2 \end{bmatrix} = 0. \tag{9}$$

We consider the difference between the reference NMO-corrected trace and traditional NMO-corrected trace $\mathbf{d} - \mathbf{NG}$ as the NMO stretching and denote it with **S**; then, we have

$$\mathbf{Sa} = \mathbf{0}. \tag{10}$$

The number of elements in **S** depends on the number of unknown coefficients in the inverse wavelet **a**. So for $\mathbf{a} = [a_0, a_1, a_2]$, we have

$$\mathbf{S} = [\mathbf{s}_0\, \mathbf{s}_1\, \mathbf{s}_2], \tag{11}$$

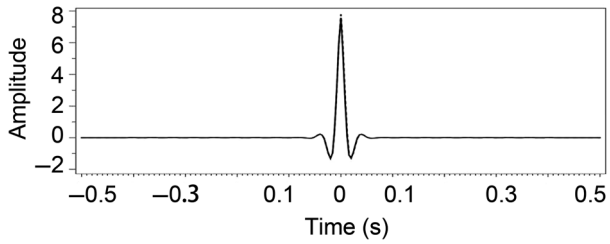

Figure 4. The wavelet (the solid curve) estimated from the synthetic gather (Figure 1a) is consistent with the ground-truth wavelet (the dashed curve) used to generate the data.

where

$$\mathbf{s}_0 = \begin{bmatrix} \mathbf{d} - \mathbf{Ng}_0 \\ \mathbf{d} - \mathbf{Ng}_1 \\ \mathbf{d} - \mathbf{Ng}_2 \end{bmatrix}, \ \mathbf{s}_1 = \begin{bmatrix} 0 \\ \mathbf{d} - \mathbf{Ng}_0 \\ \mathbf{d} - \mathbf{Ng}_1 \end{bmatrix}, \text{ and } \mathbf{s}_2 = \begin{bmatrix} 0 \\ 0 \\ \mathbf{d} - \mathbf{Ng}_0 \end{bmatrix}. \tag{12}$$

Therefore, we can calculate the inverse wavelet **a** by using equation 10. This way of estimating a wavelet through NMO stretching is inspired by the idea of estimating a wavelet through warping shifts that is proposed by Graziano and Hale (2014). It is meaningless to obtain the trivial solution $a_0 = 0$, and we can set $a_0 = 1$ to avoid this situation. We can actually set a_0 to any other constant numbers; the only difference is to scale the coefficients of the wavelet **h** by a_0. With $a_0 = 1$, we can rewrite equation 10 as

$$[\mathbf{s}_1 \mathbf{s}_2] \begin{bmatrix} a_1 \\ a_2 \end{bmatrix} = -\mathbf{s}_0. \tag{13}$$

We compute the least-squares solution of equation 13 by solving its following normal equation:

$$\begin{bmatrix} \mathbf{s}_1^\top \mathbf{s}_1 & \mathbf{s}_1^\top \mathbf{s}_2 \\ \mathbf{s}_2^\top \mathbf{s}_1 & \mathbf{s}_2^\top \mathbf{s}_2 \end{bmatrix} \begin{bmatrix} a_1 \\ a_2 \end{bmatrix} = \begin{bmatrix} \mathbf{s}_1^\top \mathbf{s}_0 \\ \mathbf{s}_2^\top \mathbf{s}_0 \end{bmatrix}. \tag{14}$$

We solve this equation by using the Cholesky decomposition to estimate the inverse wavelet **a**. With the estimated inverse wavelet **a** (Figure 3e), we further compute the wavelet **h** as shown in Figure 3f.

WNMO correction

After estimating a wavelet, we further propose a new NMO correction method called WNMO correction to reduce the NMO stretching. We introduce the entire workflow of the WNMO correction method step by step as follows (denoted by the orange arrows in Figure 3):

1) deconvolving the CMP gather (Figure 3a) with the estimated wavelet (Figure 3f) to obtain a deconvolved gather (Figure 3g)
2) flattening the deconvolved gather with an improved NMO correction method to obtain a flattened and deconvolved gather (Figure 3h)
3) convolving the flattened and deconvolved gather with the wavelet to obtain a finally corrected gather without NMO stretching (Figure 3i).

We use a synthetic example with multiple crossing hyperbolic trajectories (Figure 1a) to demonstrate the effectiveness of our WNMO correction method. We first estimate a wavelet (the solid curve in Figure 4) through the wavelet-estimating algorithm. We observe that the estimated wavelet perfectly matches the true wavelet (the dashed curve in Figure 4). We then compute the deconvolved gather (Figure 1c) using the estimated wavelet. Subsequently, we flatten the deconvolved gather (Figure 1d) with our NMO correction modified from the BMS method (Rupert and Chun, 1975). Instead of selecting a time window as one block in the original BMS method, we choose one time-sample length as one block when performing the NMO correction. By doing this, we per-

form a one-sample-length BMS NMO correction to the deconvolved gather in which the seismic events are assumed to be reflectivity impulses.

In addition, from the deconvolved gather, we are able to compute a high-resolution velocity semblance spectrum (Figure 5b), in which its energy is focused at the locations of reflectors. Compared to the semblance velocity spectrum (Figure 5a) computed from the raw gather (Figure 1a), the one (Figure 5b) computed from the deconvolved gather (Figure 1c) shows higher resolution. Based on such a high-resolution spectrum, we can not only pick accurate NMO velocities but also locate the vertical positions of reflectors. This indicates that we only need to apply NMO correction to the located reflectors in the deconvolved gather while ignoring the other vertical positions in which we do not have reflectors. By doing this, we are able to effectively reduce the NMO stretching. After applying the NMO correction to the deconvolved CMP gather (Figure 1d), we convolve the wavelet back to obtain the final NMO-corrected gather (Figure 1e). As shown in Figure 1b, the traditional NMO-corrected gather contains an obvious NMO stretching at early traveltimes and when correcting trajectory crosses. In contrast, our method (Figure 1e) significantly reduces the NMO stretching, which helps to preserve the data of shallow layers.

To further verify the effectiveness of our method, we generate a more complicated CMP gather (Figure 6a) with significantly more layers whose velocities increase linearly. This velocity model consists of a constant velocity layer of 2.1 km/s within the time range between 0 and 0.004 s, followed by multiple layers (each with a time range of 0.1 s) whose velocities linearly increase by an interval of 0.1 km/s. To test the stability of our wavelet-estimating algorithm, we use a nonzero phase wavelet to generate the synthetic data (Figure 6a). In this example, we still observe that the estimated wavelet (the solid curve in Figure 7) is consistent with the true wavelet (the dashed curve in Figure 7), which indicates that our wavelet-estimating algorithm works well for zero and nonzero phase wavelets. We then compute the deconvolved gather (Figure 6c) and the WNMO-corrected gather (Figure 6d). The results indicate that our method (Figure 6d) reduces the NMO stretching at far offsets and early traveltimes. Moreover, the reflectors in the WNMO correction are laterally more consistent and flat than the conventional one in which the NMO stretching blurs and bends the reflectors. The crossing events generate serious NMO stretching in the traditional method, whereas our method can reduce the NMO stretching. The relatively high amplitude in our method is due to the stacking of crossing positions with multiple events (Figure 6d).

Figure 8 shows the semblance velocity spectra computed from the raw CMP gather shown in Figure 6a and the deconvolved gather shown in Figure 6c, respectively. Compared to the semblance velocity spectrum (Figure 8a) computed from the raw CMP gather, the one (Figure 8b) computed from the deconvolved gather (Figure 6c) can significantly enhance the velocity-picking accuracy as depth increases, in which the energy groups are more focused on the path of the true velocity (the purple curve in Figure 8), and the energy of interferences also is better suppressed.

APPLICATION

We have shown that the wavelet-estimating method and the WNMO correction method work well in simple synthetic examples. We further apply our method to one more complicated synthetic data set generated with the Marmousi velocity model (Bourgeois et al., 1991) and two field data sets from the Northern Chicontepec Basin, Mexico, and the National Petroleum Reserve, Alaska.

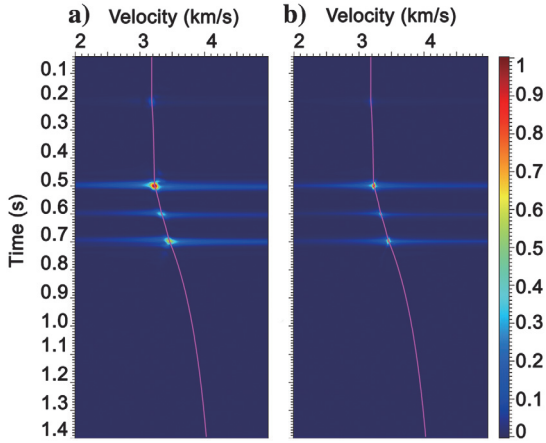

Figure 5. Semblance velocity spectrum of (a) the raw gather shown in Figure 1a and (b) the deconvolved gather shown in Figure 1c. The purple curve represents the true velocity of the gather.

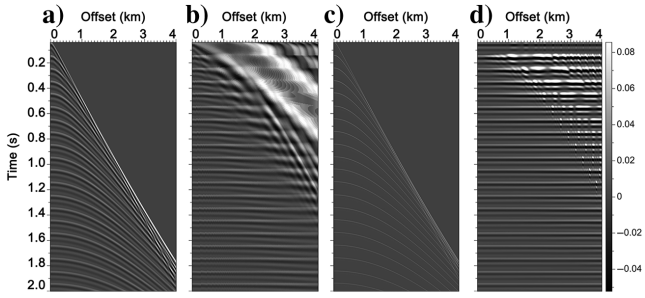

Figure 6. (a) A synthetic gather with multiple reflectors is corrected by using (b) the conventional NMO method and our method in which we first deconvolve (c) the synthetic gather and then apply the improved NMO correction method and convolve the wavelet back onto the data to obtain (d) the finally corrected gather without stretching.

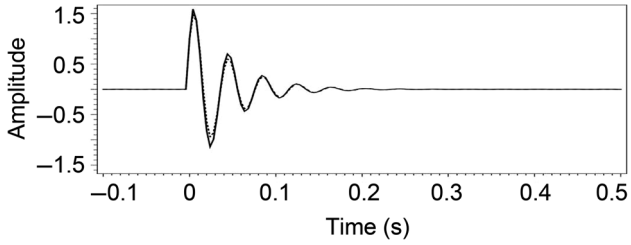

Figure 7. The wavelet (the solid curve) estimated from the synthetic gather (Figure 6a) is consistent with the ground-truth wavelet (the dashed curve) used to generate the data.

Synthetic example from the Marmousi velocity model

Figure 9a shows a CMP gather generated by using a velocity curve extracted from the Marmousi velocity model. The conventional NMO correction generates serious NMO stretching, especially at large offsets and early traveltime, as shown in Figure 9b. Such stretching reduces the resolution of thin reflectors. When velocity varies rapidly, the conventional method generates mixed reflectors as denoted by the red arrows in Figure 9b. The lateral consistency and resolution of reflectors in our result (Figure 9d) are significantly improved, especially in the time windows of 0.4–1.0 s and 1.3–1.6 s. Through the wavelet-estimating algorithm, we can also obtain the wavelet for this synthetic gather (the solid curve in Figure 10), which matches the true wavelet (the dashed curve in Figure 10) well. From the semblance velocity spectra computed from the raw CMP gather (Figure 9a) and the deconvolved gather (Figure 9b), we observe that the latter shows better focused (laterally thinner) energies and the former shows some distracting artifacts of high-energy features as denoted by the white arrows in Figure 11a.

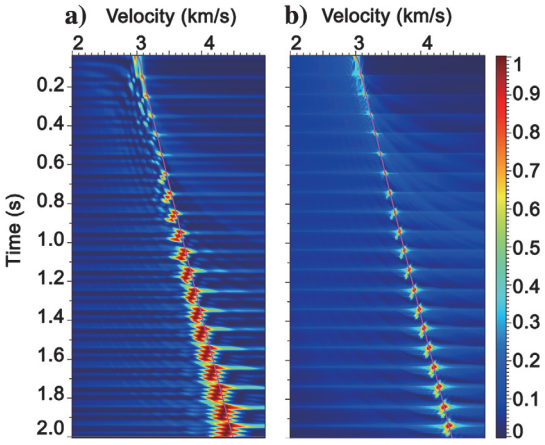

Figure 8. Semblance velocity spectra of (a) the raw gather shown in Figure 6a and (b) the deconvolved gather shown in Figure 6c. The purple curve represents the true velocity of the gather.

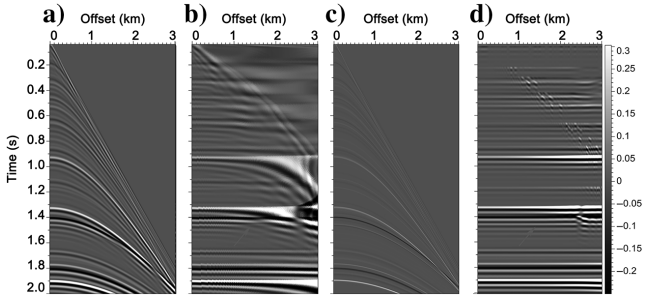

Figure 9. (a) A synthetic gather with the velocity from the Marmousi velocity model is corrected by using (b) the conventional NMO method and our method in which we first deconvolve (c) the synthetic gather and then apply the improved NMO correction method and convolve the wavelet back onto the data to obtain (d) the finally corrected gather without stretching.

The Mexico field example

Figure 12a shows one field CMP gather from the Northern Chicontepec Basin, where the target tight sand Paleocene Eocene Chicontepec Formation locates between 0.8 and 1.2 s (Sarkar, 2011). The results of the traditional NMO correction method and our WNMO correction method for the CMP gather (Figure 12a) are shown in Figure 12b and 12c, respectively. We can observe that our method can distinguish more thin reflectors and reduce the

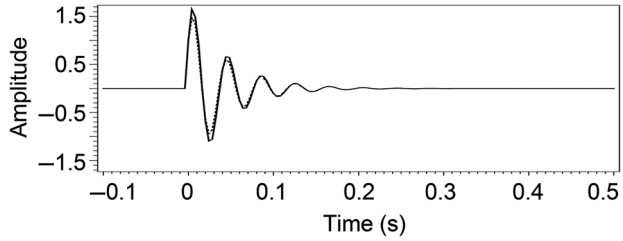

Figure 10. The wavelet (the solid curve) estimated from the synthetic gather (Figure 9a) is consistent with the ground-truth wavelet (the dashed curve) used to generate the data.

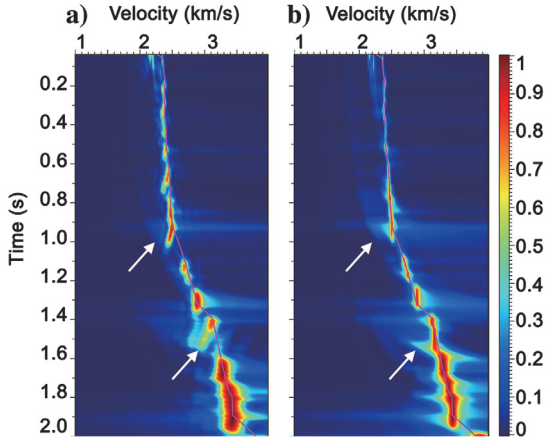

Figure 11. Semblance velocity spectra of (a) the raw gather shown in Figure 9a and (b) the deconvolved gather shown in Figure 9c. The purple curve represents the true velocity of the gather.

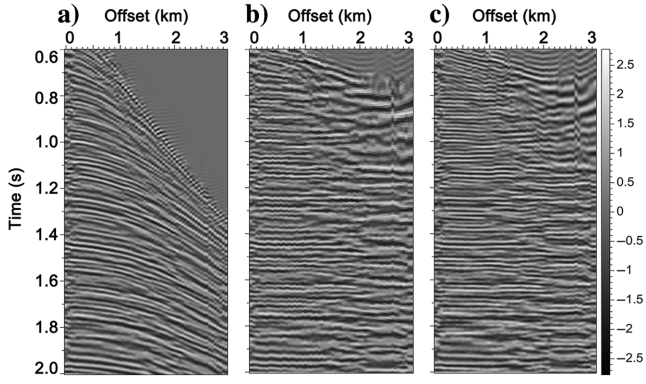

Figure 12. (a) A field gather from the Northern Chicontepec Basin is corrected by using (b) the conventional method and (c) our WNMO method.

DOI:10.1190/geo2021-0167.1

NMO stretching. In addition, we can compute the wavelet (Figure 13) for this field CMP gather.

Figure 14 illustrates the improvement of the WNMO correction method for spectrum downshifts. We compute the frequency spectra for each trace within the raw seismic gather (Figure 14a), conventional NMO-corrected gather (Figure 14b), and WNMO-corrected gather (Figure 14c). The spectra demonstrate that our WNMO correction method does not generate spectrum compression, but the conventional one downshifts the spectrum bandwidth to 60 Hz. We further stack the amplitude spectrum of limited traces to obtain the spectra of near (0–1 km), medium (1–2 km), and far (2–3 km) offset data (Figure 15). The near-offset (red) and medium-offset (blue) spectra are the same after the conventional NMO and WNMO correction, but the far-offset (green) spectra after WNMO correction preserve more high frequency than the traditional NMO correction because of the NMO stretching. To further quantitatively analyze the improvement, we compute the frequency spectra of full traces (Figure 16) in traditional NMO-corrected gather (red) and WNMO-corrected gather (blue). The effective spectra bandwidth of WNMO-corrected gather is 100% wider than the traditional one.

We horizontally stack the corrected CMP gathers with traditional methods and our method to obtain the seismic images shown in Figure 17a and 17b, respectively. Compared to the image in Figure 17a, the one in Figure 17b shows more continuous reflectors in the areas denoted by the red ellipses. In addition, the image in Figure 17b shows higher resolution reflectors, especially within the red box.

The Alaska field example

The Alaska field example is a 2D land data set provided by the U.S. Geological Survey. The original SEGY files can be downloaded from the website (U.S. Geological Survey, 1981) by searching for the line ID of 31–81. The results of traditional NMO correction and our WNMO correction method for the CMP gathers

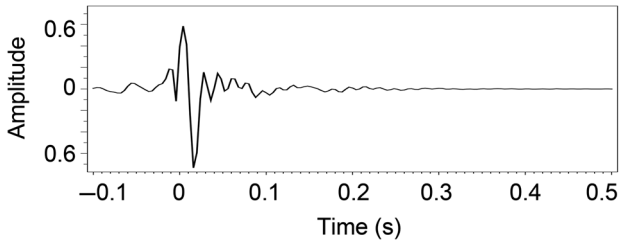

Figure 13. The wavelet estimated from the gather shown in Figure 12a.

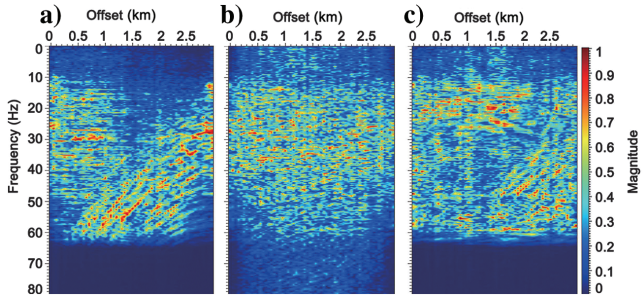

Figure 14. Fourier amplitude spectra of each trace within (a) the gather shown in Figure 12a, (b) traditional NMO-corrected gather, and (c) WNMO-corrected gather.

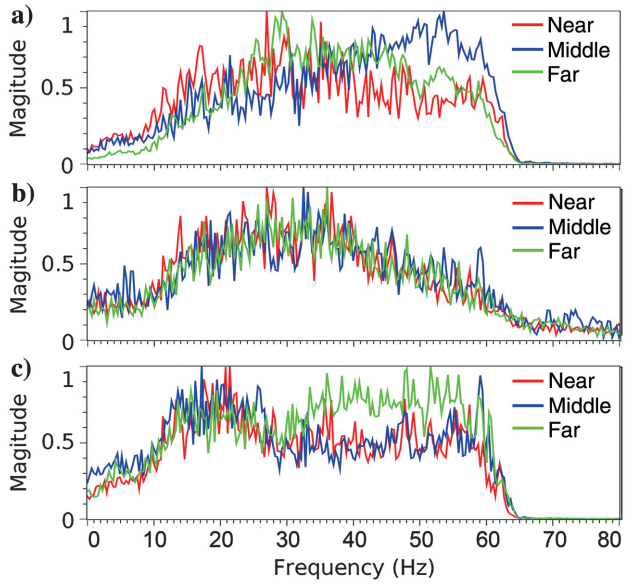

Figure 15. The near-, medium-, and far-offset amplitude spectra for the (a) input CMP gather, (b) traditional NMO-corrected gather, and (c) WNMO-corrected gather.

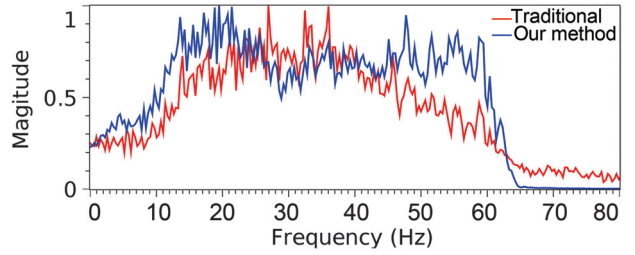

Figure 16. The amplitude spectra with all traces for traditional NMO-corrected gather (the red curve) and WNMO-corrected gather (the blue curve).

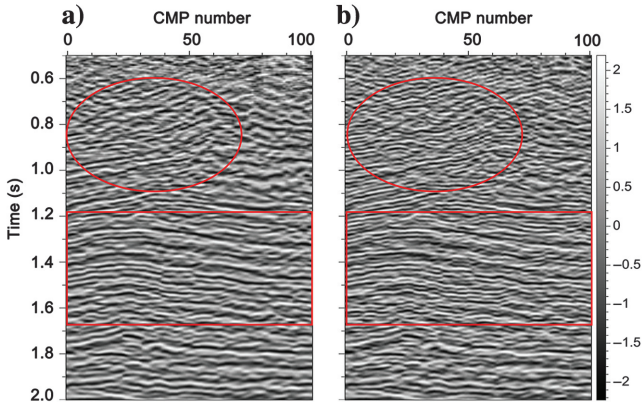

Figure 17. The seismic images in (a) and (b) are stacked from the gathers corrected by using the conventional method and our WNMO method, respectively.

(Figure 18a) are shown in Figure 18b and 18c, respectively. Our method provides a laterally better flattened CMP gather result than the traditional method, especially within the time window of 0.9–1.1 s. Our WNMO correction method not only reduces NMO stretching at the shallow layers but also provides vertically high-resolution stacked traces. For example, in Figure 18e, we can distinguish more thin layers in the stacked traces with our method (Figure 18e) within the time window of 0.5–0.6 s and 0.9–1.0 s than the traditional method (Figure 18d).

Compared with the stacked image of the traditional method (Figure 19a), our method enhances the resolution by reducing the NMO stretching. Therefore, we can observe more thin layers (especially in the shallow section) and more structural details in Figure 19b. As indicated by the two red arrows in Figure 18, the reflector discontinuities in the traditional result (Figure 19a) might be incorrectly interpreted as faults; these reflectors, however, appear continuous in our result (Figure 19b). The downlap (within the time windows of 0.75–0.88 s in Figure 19) and onlap (within the time windows of 1.08–1.35 s in Figure 19) in our result (Figure 18b) are more obvious to identify compared to the traditional one (Figure 19a). The thin layers pinch out due to lower resolution in the traditional result (denoted by the yellow arrows in Figure 19a), whereas our result can better vertically resolve these thin layers. These structural details discussed previously can be important to the following interpretation.

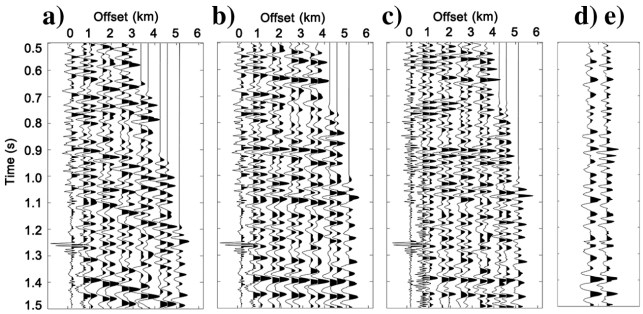

Figure 18. (a) A field gather from the National Petroleum Reserve, Alaska, is corrected by using (b) the conventional method and (c) our WNMO method. The traces shown in (d) and (e) are stacked results of (b) and (c), respectively.

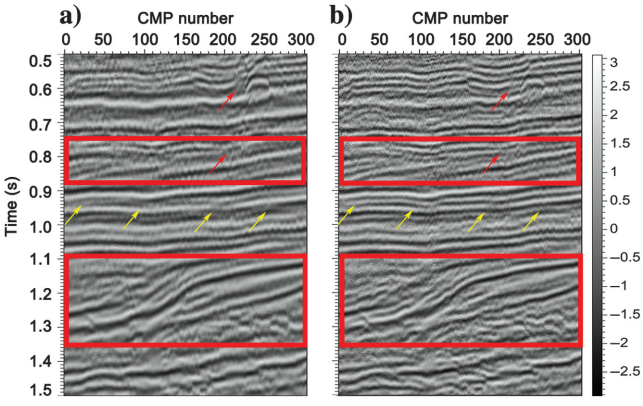

Figure 19. The seismic images in (a) and (b) are stacked from the gathers corrected by using the conventional method and our WNMO method, respectively.

DISCUSSION

We have introduced a workflow to reduce NMO stretching while at the same time estimating a wavelet. In this section, we further discuss its robustness to noise and AVO responses and its potential limitations.

Robustness to noise and AVO response

We use three more examples to test the stability of our workflow in the presence of noise and AVO responses. We first synthesize the shot gather by finite-difference forward modeling of the 2D acoustic wave equation using the velocity model in Figure 20 and then sort the shot gather into CMP gather (Figure 21a). Such a gather contains obvious AVO responses. We manually pick the rms velocity and then apply traditional NMO correction (Figure 21b) and our WNMO (Figure 21d) in which we first deconvolve the synthetic gather (Figure 21c), then apply the improved NMO correction method, and convolve the wavelet back onto the data to obtain the finally corrected gather (Figure 21d). To eliminate the AVO effect in the wavelet-estimating algorithm, we use a lateral balance filter to balance the amplitude before stacking. That is because our algorithm is based on the amplitude difference caused by the NMO stretching. The balance operator will not influence the amplitude when applying the NMO-corrected process. Because we computed the final result by convolving back the same wavelet, it will not damage the information of the final result.

Furthermore, we add 12% noise to the CMP gather (Figure 21a) to obtain a noisy CMP gather (Figure 22a) containing noise and AVO response. We also can obtain the traditional NMO-corrected gather (Figure 22b), the deconvolved CMP gather (Figure 22c), and the WNMO-corrected gather (Figure 22d). The results (Figures 21 and 22) indicate that our method can reduce the NMO stretching and preserve the information of AVO response. Such improvements will help us obtain a better image.

To further verify the robustness of our method to noise, we use the synthetic examples with various S/Ns, which are shown in Figure 23. The CMP gathers (the first row in Figure 23) are with various S/Ns of 4, 2, 1, 0.5, and 0.25. The results show that the

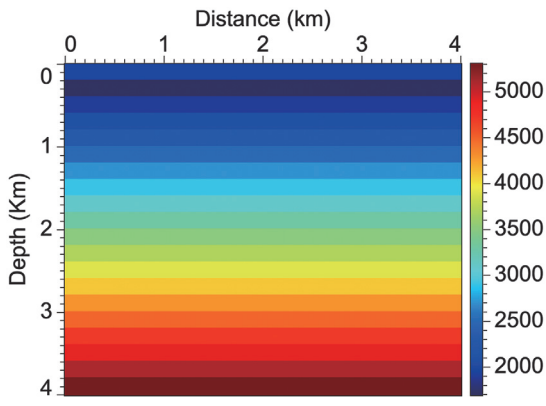

Figure 20. The velocity model used to compute the synthetic gathers of Figures 21 and 22 with finite-difference forward modeling of the 2D acoustic wave equation.

traditional method (the second row in Figure 23) and the BMS method (the third row in Figure 23) result in obvious NMO stretching. In addition, discontinuity artifacts occur at the junctions of blocks in the BMS method. In contrast, our method (the fourth row in Figure 23) better reduces the NMO stretching and preserves the information of shallow layers at far offsets for all of the examples with various S/Ns. The wavelet estimation (the sixth row in Figure 23) is indeed affected a bit by noise, but it is not highly sensitive to noise.

Limitation

Limitations still remain in the wavelet estimation and WNMO correction of our workflow. The proposed WNMO correction method consists of two main stages. The first process is wavelet estimation. The wavelet estimation algorithm is based on an assumption that the wavelet is spatially and temporally invariant. This assumption, however, is not necessarily true in practice, which remains as a limitation in our workflow. We assume the wavelet in CMP gather is spatially and temporally invariant. The wavelet used in our method is a single wavelet for all offsets. This assumption leads to violating AVO principles. So our method can only estimate a rough and average wavelet for all offsets. Fortunately, it is acceptable for the purpose of reducing the NMO stretching. Without an ideally estimated wavelet, we cannot obtain perfect reflectivity spikes when applying it to deconvolve the CMP gather. However, field examples show that this process is still helpful in reducing the NMO stretching and improving the resolution of a stacked image.

Another assumption in the wavelet estimation is that the ideal NMO-corrected gather can be replaced by stacking the traditional NMO-corrected traces, which could be another limitation of our method because we cannot obtain an ideal NMO-corrected gather in practice. This means that the reference NMO-corrected gather used to estimate the wavelet is not a perfect result, but it typically contains artifacts. These artifacts will influence the wavelet estimation in our method. However, we can reduce the influence of the artifacts by carefully choosing the NMO-corrected traces to stack for the reference. Specifically, we stack only the near-offset traces without significant NMO stretching to compute the reference for estimating the wavelet. By doing this, we are able to estimate acceptable wavelets as shown in multiple synthetic and field examples (including simple and complex velocity models).

Our modified BMS NMO correction requires first locating the positions of reflectors, which could be challenging in complex field examples. Accurately locating the reflector positions requires a high-resolution semblance velocity spectrum (like those in Figures 5, 8, and 11) computed from an ideally deconvolved CMP gather. However, the velocity picking and deconvolution are generally done before NMO correction and these steps are repeated in our workflow. To obtain a better image, it is acceptable to perform these methods, which do not cost much computation. In a complex field example in which we cannot accurately locate the reflector positions, we may directly perform the traditional NMO correction to the deconvolved CMP gather in our workflow to preserve the seismic amplitude. When the wavelet is not 100% accurate, the final NMO-corrected results still show the advantage of reducing the NMO stretching and the semblance velocity spectrum can still enhance the velocity-picking accuracy as depth increases, in which the energy groups are more focused on the path of true velocity. These points can be proven in multiple examples as shown previously.

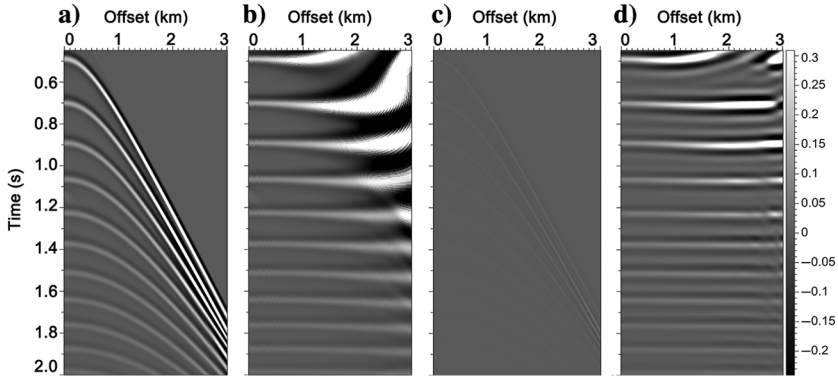

Figure 21. (a) A synthetic gather is synthesized by finite-difference forward modeling of the 2D acoustic wave equation using the velocity model in Figure 20. Such a gather contains an obvious AVO response. It is corrected by using (b) a conventional NMO method and our method in which we first deconvolve (c) the synthetic gather and then apply the improved NMO correction method and convolve the wavelet back onto the data to obtain (d) the finally corrected gather. Such a result indicates the stability of our method in the presence of AVO responses.

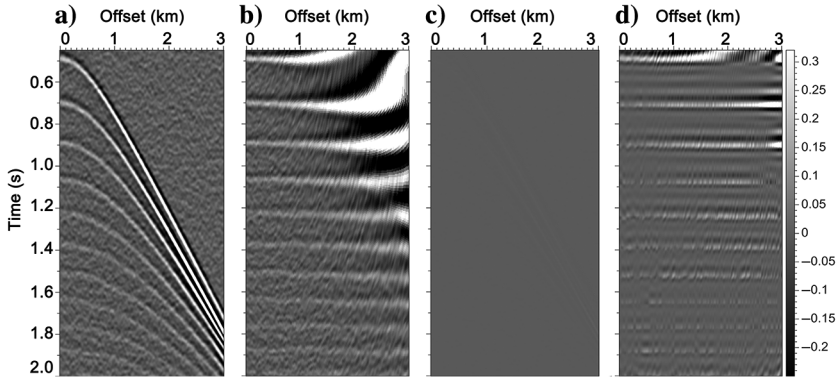

Figure 22. (a) A noisy synthetic gather is synthesized by finite-difference forward modeling of the 2D acoustic wave equation using the velocity model in Figure 20. Such a gather contains an obvious AVO response. It is corrected by using (b) a conventional NMO method and our method in which we first deconvolve (c) the synthetic gather and then apply the improved NMO correction method and convolve the wavelet back onto the data to obtain (d) the finally corrected gather. Our result can reduce the NMO stretching, and such a result indicates the stability of our method in the presence of noise and AVO responses.

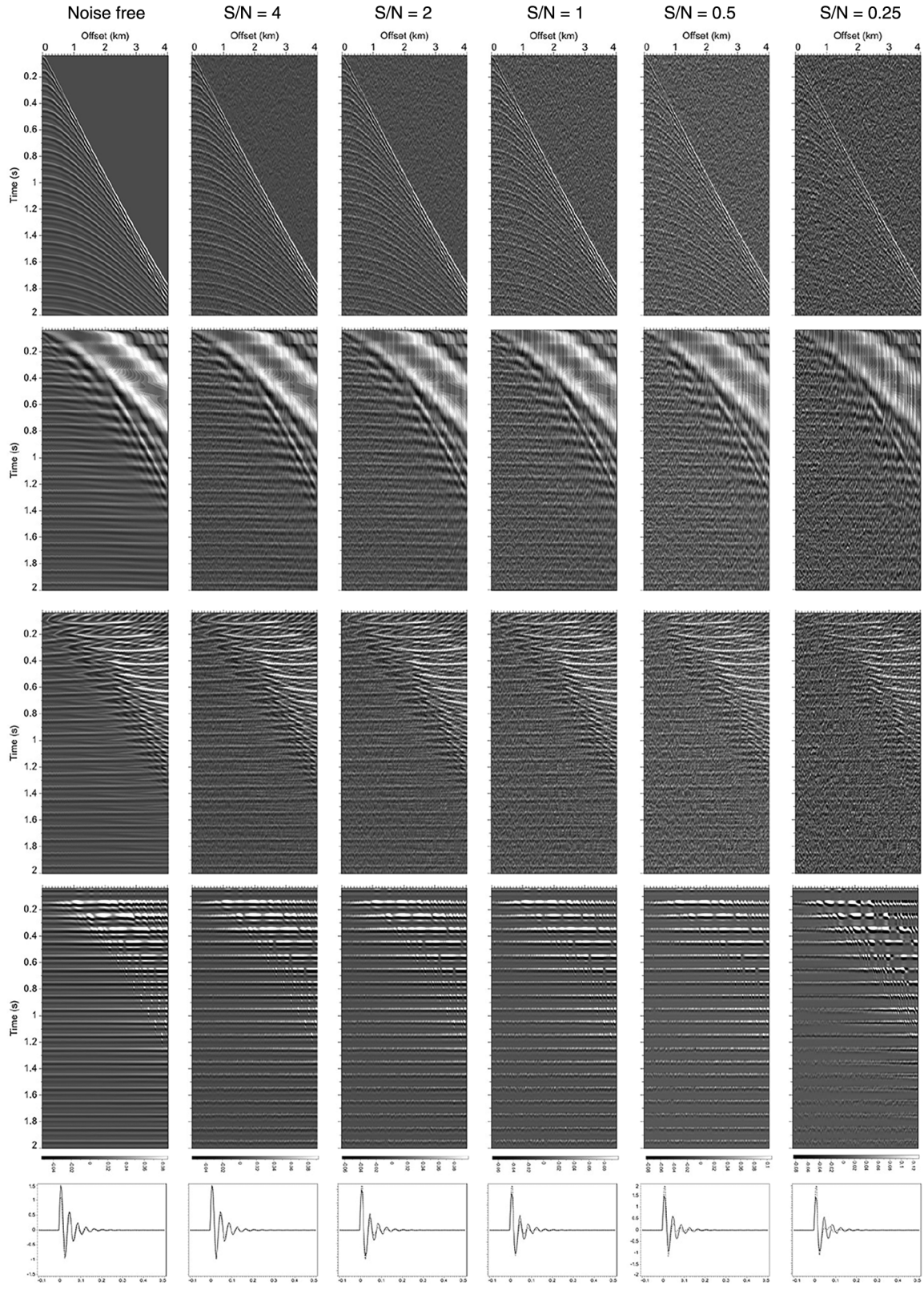

Figure 23. The first row is the CMP gathers with various S/Ns including noise free, 4, 2, 1, 0.5, and 0.25. The second row is the conventional NMO-corrected gathers method. The third row is the result of the BMS method, in which the NMO stretching is not well eliminated and discontinuity artifacts occur at the junction of the blocks. The fourth row is the results of our method, in which the NMO stretching is well reduced. Compared with the traditional method and the BMS method, our method improves the continuity of the reflectors and attenuates some noise. The wavelet (the dashed curve) estimated from the above CMP gather and the ground-truth wavelet (the solid curve) are shown in the fifth row, respectively. The estimated wavelets are basically comprised of the true wavelets.

CONCLUSION

We have proposed a new NMO correction method which we call the WNMO correction method. Our method contains two processes: first, a wavelet-estimating algorithm using NMO stretching, and second, a new NMO correction method including (1) deconvolving the input gather with the estimated wavelet, (2) flattening the deconvolved gather with an improved NMO correction method, and (3) convolving the flat deconvolved gather with the wavelet to obtain the improved NMO-corrected gather. In the improved NMO correction, we first detect the reflector positions from a high-resolution semblance velocity spectrum computed from a deconvolved CMP gather. We then apply the BMS NMO correction to only the detected reflectors to avoid NMO stretching. By using our WNMO correction method, we can significantly reduce the NMO stretching. The tests on synthetic and field data indicate that our method can preserve more information of the shallow layers at far offsets, improve the continuity of layers in the NMO-corrected gather, and reduce the frequency spectrum compression while performing NMO correction. With our wavelet-estimating algorithm, we can obtain the wavelet through NMO stretching. In addition, we can pick a more accurate velocity from a high-resolution semblance velocity spectrum computed from a deconvolved CMP gather.

ACKNOWLEDGMENTS

We thank the editor-in-chief, J. Etgen, an anonymous assistant editor, and the associate editor, M. Nagizadeh, for their valuable remarks. We also thank the anonymous reviewers and Z. Hu for their suggestions. This work is financially supported by the National Key R&D Program of China under the grant no. 2021YFA0716903.

DATA AND MATERIALS AVAILABILITY

Data associated with this research are available and can be obtained by contacting the corresponding author.

REFERENCES

Abedi, M. M., and M. A. Riahi, 2016, Nonhyperbolic stretch-free normal moveout correction: Geophysics, **81**, no. 6, U87–U95, doi: 10.1190/geo2016-0078.1.
Alkhalifah, T., 1997, Seismic data processing in vertically inhomogeneous TI media: Geophysics, **62**, 662–675, doi: 10.1190/1.1444175.
Alkhalifah, T., 1998, Acoustic approximations for processing in transversely isotropic media: Geophysics, **63**, 623–631, doi: 10.1190/1.1444361.
Barnes, A. E., 1992, Another look at NMO stretch: Geophysics, **57**, 749–751, doi: 10.1190/1.1443289.
Biondi, E., E. Stucchi, and A. Mazzotti, 2014, Nonstretch normal moveout through iterative partial correction and deconvolution: Geophysics, **79**, no. 4, V131–V141, doi: 10.1190/geo2013-0392.1.
Bolshykh, S. F., 1956, About an approximate representation of the reflected wave traveltime curve in the case of a multi-layered medium: Applied Geophysics (in Russian), **5**, 3–15.
Bourgeois, A., M. Bourget, P. Lailly, M. Poulet, P. Ricarte, and R. Versteeg, 1991, The Marmousi experience: Proceedings of the 1990 EAEG Workshop, Marmousi, Model and Data, 5–16.
Brouwer, J., 2002, Improved NMO correction with a specific application to shallow-seismic data: Geophysical Prospecting, **50**, 225–237, doi: 10.1046/j.1365-2478.2002.00310.x.
Buchholtz, H., 1972, A note on signal distortion due to dynamic (NMO) corrections: Geophysical Prospecting, **20**, 395–402, doi: 10.1111/j.1365-2478.1972.tb00642.x.
Castle, R. J., 1994, A theory of normal moveout: Geophysics, **59**, 983–999, doi: 10.1190/1.1443658.
de Bazelaire, E., 1988, Normal moveout revisited: Inhomogeneous media and curved interfaces: Geophysics, **53**, 143–157, doi: 10.1190/1.1442449.
de Bazelaire, E., and J. R. Viallix, 1994, Normal moveout in focus: Geophysical Prospecting, **42**, 477–499.
Dix, C., 1955, Seismic velocity from surface measurements: Geophysics, **20**, 68–86, doi: 10.1190/1.1438126.
Downton, J., and C. Ursenbach, 2006, Linearized amplitude variation with offset (AVO) inversion with supercritical angles: Geophysics, **71**, no. 5, E49–E55, doi: 10.1190/1.2227617.
Drufuca, G., and A. Mazzotti, 1995, Ambiguities in AVO inversion of reflections from gassand: Geophysics, **60**, 134–141, doi: 10.1190/1.1443740.
Dunkin, J. W., and F. K. Levin, 1973, Effect of normal moveout on a seismic pulse: Geophysics, **38**, 635–642, doi: 10.1190/1.1440363.
Fomel, S., and A. Stovas, 2010, Generalized nonhyperbolic moveout approximation: Geophysics, **75**, no. 2, U9–U18, doi: 10.1190/1.3334323.
Graziano, C., and D. Hale, 2014, Wavelets and warping PS seismic images: 84th Annual International Meeting, SEG, Expanded Abstracts, 1848–1852, doi: 10.1190/segam2014-0362.1.
Hicks, G., 2001, Removing NMO stretch using the Radon and Fourier-Radon transforms: 63rd Annual Conference and Exhibition, EAGE, Extended Abstracts, A-18, doi: 10.3997/2214-4609-pdb.15.A-18.
Hilterman, F., and C. V. Schuyver, 2003, Seismic wide-angle processing to avoid NMO stretch: 73rd Annual International Meeting, SEG, Expanded Abstracts, 215–218, doi: 10.1190/1.1817768.
Kazemi, N., and M. D. Sacchi, 2014, Sparse multichannel blind deconvolution: Geophysics, **79**, no. 5, V143–V152, doi: 10.1190/geo2013-0465.1.
Lichman, E., 1999, Automated phase-based moveout correction: 69th Annual International Meeting, SEG, Expanded Abstracts, 1150–1153, doi: 10.1190/1.1820706.
Masoomzadeh, H., P. Barton, and S. Singh, 2010, Nonstretch moveout correction of long-offset multichannel seismic data for subbasalt imaging: Example from the North Atlantic: Geophysics, **75**, no. 4, R83–R91, doi: 10.1190/1.3443579.
Miller, R., 1992, Normal moveout stretch mute on shallow-reflection data: Geophysics, **57**, 1502–1507, doi: 10.1190/1.1443217.
Noah, J., 1996, NMO stretch and subtle traps: The Leading Edge, **15**, 345–347, doi: 10.1190/1.1437335.
Perez, G., and K. Marfurt, 2007, Improving lateral and vertical resolution of seismic images by correcting for wavelet stretch in common-angle migration: Geophysics, **72**, no. 6, C95–C104, doi: 10.1190/1.2781619.
Perroud, H., and M. Tygel, 2004, Nonstretch NMO: Geophysics, **69**, 599–607, doi: 10.1190/1.1707080.
Prieux, V., G. Lambaré, S. Operto, and J. Virieux, 2013, Building starting models for full waveform inversion from wide-aperture data by stereotomography: Geophysical Prospecting, **61**, 109–137, doi: 10.1111/j.1365-2478.2012.01099.x.
Roberts, G., 2000, Wide-angle AVO: 70th Annual International Meeting, SEG, Expanded Abstracts, 134–137, doi: 10.3997/2214-4609-pdb.28.C34.
Rupert, G. B., and J. H. Chun, 1975, The block move sum normal moveout correction: Geophysics, **40**, 17–24, doi: 10.1190/1.1440511.
Sarkar, S., 2011, Depositional history and reservoir characteristics of structurally confined foredeep turbidites, Northern Chicontepec Basin, Mexico: Ph.D. thesis, The University of Oklahoma.
Shatilo, A., and F. Aminzadeh, 2000, Constant normal-moveout (CNMO) correction: A technique and test results: Geophysical Prospecting, **48**, 473–488, doi: 10.1046/j.1365-2478.2000.00190.x.
Taner, M., and F. Koelher, 1969, Velocity spectra-digital computer derivation applications of velocity function: Geophysics, **34**, 859–881, doi: 10.1190/1.1440058.
Trickett, S., 2003, Stretch-free stacking: 73rd Annual International Meeting, SEG, Expanded Abstracts, 2008–2011, doi: 10.1190/1.1817723.
Ursin, B., and A. Stovas, 2006, Traveltime approximations for a layered transversely isotropic medium: Geophysics, **71**, no. 2, D23–D33, doi: 10.1190/1.2187716.
U.S. Geological Survey, 1981, Alaska 2D land line 31-81, https://certmapper.cr.usgs.gov/data/apps/npra/, accessed 31 December 2019.
Xu, G., H. Liu, L. Tong, and T. Kailath, 1995, A least-squares approach to blind channel identification: IEEE Transactions on Signal Processing, **43**, 2982–2993, doi: 10.1109/78.476442.
Zhang, B., K. Zhang, S. Guo, and K. Marfurt, 2012, Nonstretching NMO correction of prestack time-migrated gathers using a matching-pursuit algorithm: Geophysics, **78**, no. 1, U9–U18, doi: 10.1190/geo2011-0509.1.

Biographies and photographs of the authors are not available.